Transient response of the Earth's magnetosphere to a localized density pulse in the solar wind: Simulation of traveling convection vortices

Ryuho Kataoka,[1] Hiroshi Fukunishi,[1] Shigeru Fujita,[2] Takashi Tanaka,[3] and Masahiro Itonaga[4]

Received 14 October 2003; revised 21 November 2003; accepted 23 January 2004; published 6 March 2004.

[1] We investigate the transient response of the Earth's magnetosphere-ionosphere system to a localized density pulse in the solar wind using a magnetohydrodynamic simulation. The simulated ionospheric disturbances exhibit many properties similar to those observed during traveling convection vortices (TCVs). The simulated TCVs are driven by pairs of field-aligned currents. The generation mechanisms of the field-aligned currents in the magnetosphere are evaluated in terms of a wave equation of field-aligned currents. The source current is the inertial current associated with in-out plasma acceleration in the magnetosphere near the impact region. The inertial current is converted into the field-aligned current off from the equatorial region via the curvilinear effect. The inhomogeneous effect also generates the field-aligned current near the inner equatorial region where the sharp gradient of Alfvén speed exists. *INDEX TERMS:* 2784 Magnetospheric Physics: Solar wind/magnetosphere interactions; 2708 Magnetospheric Physics: Current systems (2409); 2753 Magnetospheric Physics: Numerical modeling; 2724 Magnetospheric Physics: Magnetopause, cusp, and boundary layers; *KEYWORDS:* traveling convection vortices, global MHD simulation, field-aligned currents

Citation: Kataoka, R., H. Fukunishi, S. Fujita, T. Tanaka, and M. Itonaga (2004), Transient response of the Earth's magnetosphere to a localized density pulse in the solar wind: Simulation of traveling convection vortices, *J. Geophys. Res.*, *109*, A03204, doi:10.1029/2003JA010287.

1. Introduction

[2] There are several kinds of interactions between the solar wind and the Earth's magnetosphere, such as dayside reconnection, pressure pulses, and Kelvin-Helmholtz instabilities. These interaction processes cause transient electromagnetic disturbances in the dayside magnetosphere and drive field-aligned currents flowing into and out of the dayside ionosphere. The field-aligned currents convey electromagnetic energy from the magnetosphere to the ionosphere. The power supply into the ionosphere via each transient is typically small ($\sim$1 GW) compared with substorms (>10 GW) or storms (>100 GW). However, disturbances of the dayside magnetosphere and ionosphere are sometimes governed by the accumulation of such transients when the transients constantly arise with continual solar wind disturbances. Therefore it is essential to investigate these transients themselves for understanding the energetics of the dayside magnetosphere and ionosphere.

[3] Among these transients, traveling convection vortices (TCVs) [*Friis-Christensen et al.*, 1988; *Glassmeier et al.*, 1989] are known as the best clue to elucidate such a transient response of the dayside magnetosphere because of their solitary feature. TCVs are identified as one or more east-west aligned pairs of oppositely directed flow vortices which propagate through the dayside ionosphere eastward or westward at speeds of 3–10 km/s over 5–15 min in magnetic latitudes of 70°–80°. Each vortex has a spatial scale of 1000–2000 km, such that twin vortices encompass several hours in local time.

[4] In spite of their distinct property, the generation mechanism of TCVs is still under debate. Since recent observations suggest that small-scale pressure pulses generated within the foreshock is the most probable cause of TCVs [*Sibeck et al.*, 2003; *Murr and Hughes*, 2003], we introduce how the field-aligned currents driving TCVs are generated due to a localized pressure pulse impinging upon the magnetopause. As summarized by *Cowley* [2000], there are at least three generation mechanisms of the field-aligned currents. *Glassmeier* [1992] (G92) showed the generation of one field-aligned current at each end of the perturbed region based on the continuity of the perturbed magnetopause current. *Kivelson and Southwood* [1991] (KS91) predicted a pair of field-aligned currents at each end by considering flow shear due to in-out boundary motions. The dominant source current is the diamagnetic current and the inertia current for the G92 model and for the KS91 model, respectively, although the source region is the magnetopause in both models. On the other hand, *Lühr et al.* [1996] (L96) suggested that field-aligned currents are associated with the divergence of the inertia current at sharp density

[1]Department of Geophysics, Tohoku University, Sendai, Japan.
[2]Meteorological College, Kashiwa, Japan.
[3]Graduate School of Sciences, Kyushu University, Fukuoka, Japan.
[4]Faculty of Education, Yamaguchi University, Yamaguchi, Japan.

0148-0227/04/2003JA010287

gradient on the inner edge of the low-latitude boundary layer (LLBL).

[5] Recently, global magnetohydrodynamic (MHD) simulation has been a powerful tool for investigating magnetospheric phenomena. TCVs have also been studied by the MHD simulation. *Lysak and Lee* [1992] simulated the transient response of the dipole magnetosphere to pressure pulses using a set of linearized cold plasma MHD equations. Their result showed that vortex structures tend to form on field lines resonant with the source frequency. *Slinker et al.* [1999] are the first researchers who investigated the response of the ionosphere to a density pulse in the solar wind using a global MHD simulation. They reproduced pairs of ionospheric convection vortices traveling away from noon, and showed the corresponding plasma convection in the magnetospheric equatorial region. On the other hand, *Chen et al.* [2000] investigated the response of the magnetosheath and the magnetosphere to a pressure enhancement accompanied by a solar wind tangential discontinuity using a global MHD simulation. They showed that tailward traveling twin vortices and shear Alfvén waves arise in the dayside magnetosphere.

[6] All of the previous simulation models [*Lysak and Lee*, 1992; *Slinker et al.*, 1999; *Chen et al.*, 2000] form symmetrical vortices across the noon-midnight meridian because they dealt with vertical impinging of the uniform solar wind density pulse to the magnetopause. However, observed TCVs do not show such dawn-dusk symmetry. Also, statistical studies show the dominant occurrence of the morning TCVs [e.g., *Lanzerotti et al.*, 1991; *Kataoka et al.*, 2003b]. In addition, pressure pulses localized in the dawn sector may be a more realistic solar wind input in terms of foreshock cavities [*Sibeck et al.*, 2001]. In this paper, we perform a simulation of magnetospheric and ionospheric response to such a localized density pulse in the solar wind.

2. Simulation Model

[7] The numerical technique used in this study was developed by *Tanaka* [1994, 1995, 2000a, 2000b]. The finite volume (FV) total-variation diminishing (TVD) scheme is employed to solve the three-dimensional MHD equations in a solar wind-magnetosphere-ionosphere system. The boundary conditions and the grid system are explained in detail by *Tanaka* [2000a]. The outer and inner boundaries for the simulation are at 200 R_E and 3 R_E from the center of the Earth. Simulation results at 3 R_E are mapped along dipole field lines to the ionosphere at 1 R_E. The inner boundary condition is given by current continuity and continuity of plasma flows tangential to the ionosphere. The height-integrated ionospheric conductivity is given by considering the effects of solar EUV, diffuse auroral precipitation, and upward field-aligned current. The grid system within the dayside magnetosphere is basically a spherical coordinate system. The spatial resolution in the dayside magnetosphere is $\sim$0.25 R_E in radial direction, $\sim$1.0° in latitude, and $\sim$1.5° in longitude.

[8] Initial conditions are basically the same as the ones given by *Fujita et al.* [2003] except for the localized compression of the magnetosphere. The cylindrical density enhancement with 2 R_E radius aligned with Z axis is superposed upstream of the prenoon magnetosphere at $Y = -5$ R_E, where X and Z axes denote the sunward and the northward direction, respectively, and Y completes the orthogonal triad. The solar wind density is set to be 25/cc and 10/cc inside and outside of the column, respectively. The solar wind velocity is 350 km/s in the negative X direction, and the corresponding dynamic pressure is 5.1 nPa and 2.0 nPa inside and outside of the column, respectively. In order to investigate the power supply due to the density impact regardless of dayside reconnection effects, IMF is set to be northward, IMF (B_X, B_Y, B_Z) = (0.0, 2.5, 4.3) nT. The time axis is selected so that the density column appears in the upstream region of the Earth's bow shock ($X = 18$ R_E at 0.0 min).

[9] Figure 1 shows the time evolution of the density distribution in the magnetospheric equatorial plane for the time interval from 2.1 min to 7.0 min to overview simulated plasma disturbances in the magnetosphere. We close up the prenoon sector because of no significant disturbances in the postnoon sector. Magnetopause location is shown with a white line in each panel. The density column arrives at the magnetopause at 2.1 min with a peak density of >50/cc in the magnetosheath. The density column leads to a ripple propagating antisunward along the magnetopause after 3.0 min. Both the density column and the magnetopause ripple decay as traveling antisunward. The azimuthal extent of the magnetopause ripple ($\sim$5 R_E) is comparable to that expected from observations of small-scale pressure pulses [e.g., *Sibeck et al.*, 2003].

3. Ionospheric Disturbances

[10] We first show how our experiment reproduces ionospheric signatures of TCVs. Figure 2 shows temporal variations of field-aligned currents every 1 min in the latitude range higher than 60° in the ionosphere for the time interval from 2.1 min to 7.0 min. Field-aligned currents shown by red and blue colors are downward (into the ionosphere, positive) and upward (out of the ionosphere, negative), respectively. Superposed contour lines show the ionospheric electric potential. The electric potential corresponds to the ionospheric convection vortices. In the Northern Hemisphere, ionospheric plasma flows clockwise and counterclockwise along the negative and positive contour lines, respectively. The first panel at 2.1 min shows a quasi-steady current system and a corresponding convection pattern under northward IMF condition as explained by *Tanaka* [1999]. There are no signals associated with the density impact at 2.1 min. In order to demonstrate the perturbed features clearly, five panels after 2.1 min show the deviations of field-aligned currents and potential from those at 2.1 min.

[11] At 3.0 min, a pair of clockwise (negative potential) and counterclockwise (positive potential) vortices appears at latitudes of $\sim$70° centered around 0800–0900 and 1100–1300 hour LT, respectively. In the time interval 4.0–6.0 min, the positive potential peak moves from 1100 LT to 0900 LT at the latitude of $\sim$75°, resulting in the averaged propagation speed of $\sim$7 km/s. At 5.0 min a new clockwise vortex (negative potential) appears centered around 1100–1300 LT. In the interval of 6.0–7.0 min, the negative potential peak moves from 1200 LT to 1100 LT at the

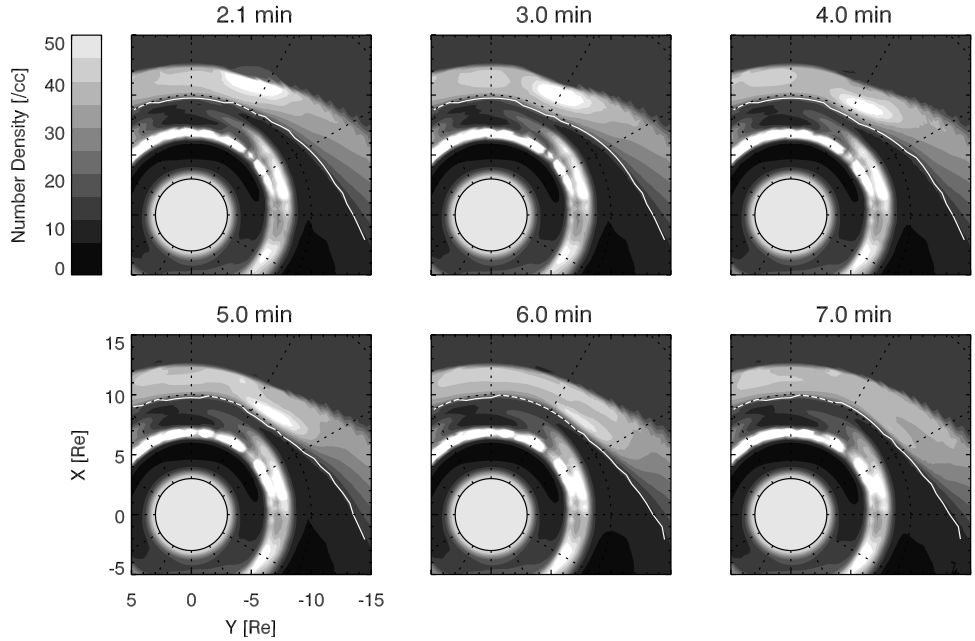

Figure 1. Equatorial maps of plasma density in the prenoon sector for the time interval from 2.1 min to 7.0 min. The contour interval is 5/cc. Magnetopause location is shown as a white line in each panel.

latitude of ~75°, giving an averaged propagation speed of ~7 km/s. The propagation speeds of the simulated TCVs are comparable with magnetometer observations [*Murr et al.*, 2002; *Kataoka et al.*, 2001, 2002, 2003a; *Amm et al.*, 2002]. The skew of the simulated TCVs as moving away from noon is also consistent with magnetometer observations [e.g., *Friis-Christensen et al.*, 1988; *Lühr and Blawert*, 1994; *Moretto et al.*, 1997; *Murr et al.*, 2002].

[12] Let us consider the field-aligned currents that generate the ionospheric electric field of TCVs. At 3.0 min, a pair of upward and downward field-aligned currents appears at latitudes of ~70° centered around 0800–0900 and 1100–1300 LT, respectively. This is essentially the same signature as the preliminarily impulse phase explained in detail by *Fujita et al.* [2003] except for a less LT extent due to the localized compression. At 4.0–5.0 min, when a pair of field-aligned currents grows and shifts toward higher latitudes and westward, a new upward field-aligned current appears at latitudes lower than the area of the preceding downward field-aligned current

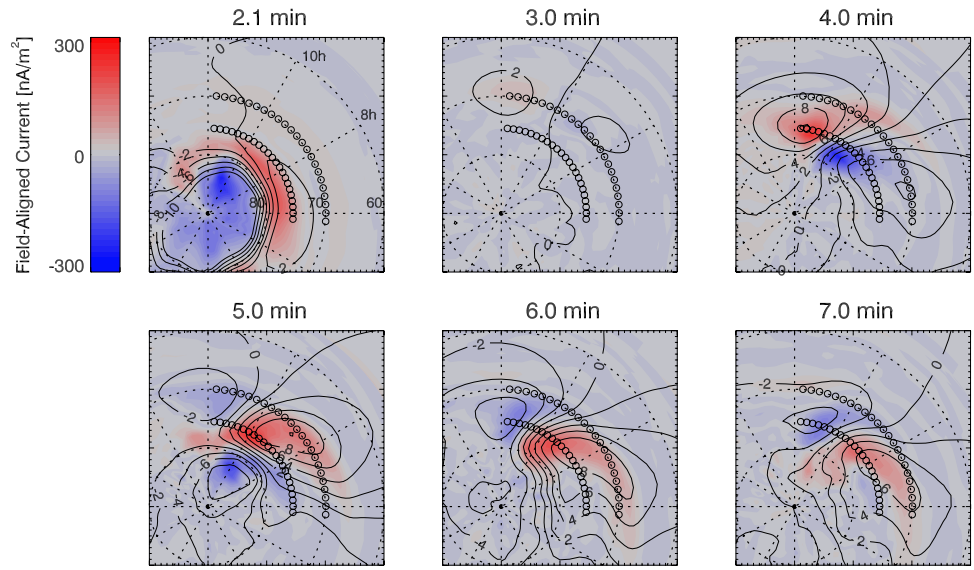

Figure 2. Time variation of field-aligned currents (colors) at the ionosphere level and that of the ionospheric electric potential (contour lines) in the prenoon sector for the time interval from 2.1 min to 7.0 min and in the latitude range higher than 60°. Red and blue colors indicate downward and upward field-aligned currents, respectively. The contour interval is 2 kV for the potential. Circles indicate the footprint positions of magnetic field lines shown in Figures 4 and 5.

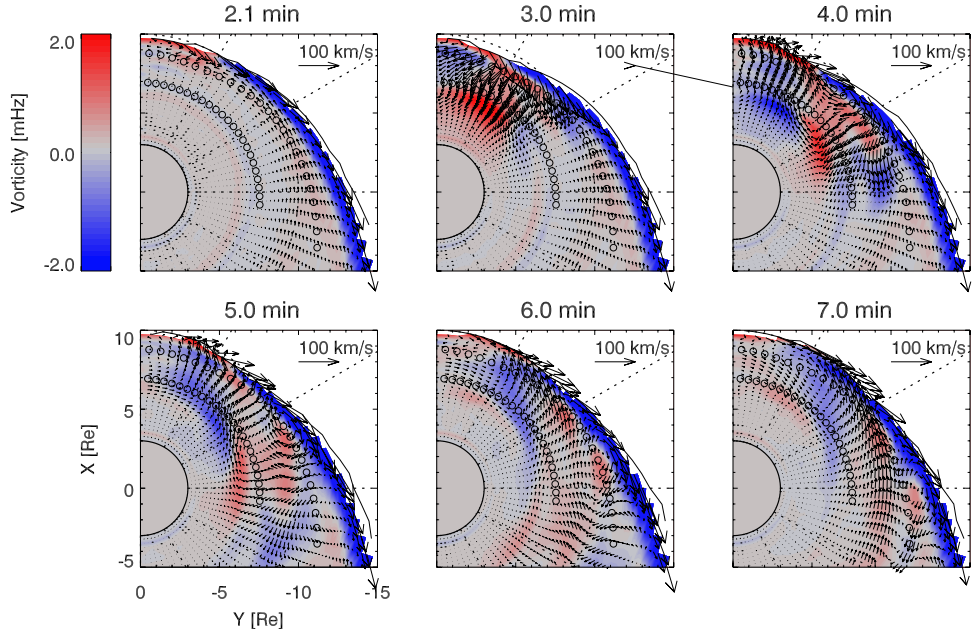

Figure 3. Maps of magnetospheric plasma flows (arrows) and vorticities (colors) on the equatorial plane in the prenoon sector for the simulation time interval from 2.1 min to 7.0 min. Vectors are drawn in the region where magnetic field is almost perpendicular to the equatorial plane. Chains of circles indicate the equatorial intersects of magnetic field lines shown in Figures 4 and 5.

centered around 1100–1300 LT. After 6.0 min, a new pair of preceding downward and trailing upward field-aligned currents shifts westward with less distinguished latitudinal motion. In past observational studies, field-aligned current densities associated with TCVs have been estimated to be of the order of 1 $\mu A/m^2$ [*Glassmeier et al.*, 1989; *Glassmeier*, 1992; *Lanzerotti et al.*, 1991; *Lühr and Blawert*, 1994; *Lühr et al.*, 1996; *Murr et al.*, 2002; *Amm et al.*, 2002]. The maximum density of a pair of field-aligned currents in our simulation is $\sim$0.3 $\mu A/m^2$. The field-aligned currents are strong near the poleward and the rear edge of the simulated TCV. This is also consistent with the picture obtained from recent observations [*Kataoka et al.*, 2001; *Amm et al.*, 2002]. In other words, the TCV centers tend to be located equatorward of the field-aligned current peaks. This could attribute to the fact that TCVs are often mapped well inside of the magnetopause [*Moretto and Yahnin*, 1998], while sometimes the source region was located much closer to the magnetopause [*Kataoka et al.*, 2001]. Thus it is concluded that the simulated ionospheric disturbances exhibit the common properties similar to those observed during TCVs.

4. Magnetospheric Disturbances

[13] From the simulation result of the ionospheric response, it is revealed that the localized density pulse in the solar wind is a possible source of TCVs. Therefore the numerical results deserve to be analyzed in detail for investigation of magnetospheric plasma processes associated with TCVs. In order to understand how the field-aligned currents driving the simulated TCVs are generated in the magnetosphere, we first investigate the magnetospheric plasma disturbances caused by the localized density pulse. Bearing in mind that magnetospheric plasma flows and vorticities convey fundamental information about the magnetosphere-ionosphere system, we show their temporal variations in the equatorial plane in Figure 3. Vectors of perpendicular plasma flows are shown as black arrows. Red and blue colors show positive and negative vorticities, respectively. The positive and negative vorticities correspond to downward (into the ionosphere) and upward (out of the ionosphere) field-aligned currents, respectively. The inner and outer chains of circles in Figure 3 are the equatorial intersects of the field lines originated from the ionosphere at latitudes of 70° and 75°, respectively. The ionospheric ends of the 70° and 75° field lines are also shown as chains of circles in Figure 2.

[14] In the magnetosphere at 2.1 min just before the impact, there are weak sunward flows in the magnetosphere and strong antisunward flows in the magnetopause region. These flows are associated with quasi-steady magnetospheric plasma convection under northward IMF condition as explained by *Tanaka* [1999]. At 3.0 min, the density impact impinging onto the magnetopause invokes earthward flows around the perturbed region. This is a signature of compressional disturbance. The flows turn toward antisunward in the front region of the disturbance in the inner magnetosphere ($L < 6$). There appears a flow shear, in other words, the Alfvén mode disturbance with a field-aligned current is produced. Actually, we confirmed that this is the mode conversion from the compressional wave to the shear Alfvén wave by the same way as discussed by *Fujita et al.* [2003]. At 4.0 min, these antisunward flows turn sunward to induce a flow shear in reverse sense. The same type of the shear structure was first reported by *Slinker et al.* [1999]. The flow shear fades away gradually after 5.0 min as propagating antisunward.

[15] Basically, the electric charge, equivalent of the vorticity in the first approximation, is transmitted to the ionosphere as the electric potential with the Alfvén transit time delay because the energy is conveyed by shear Alfvén waves with field-aligned currents. There is 20–60 s (80–140 s) propagation time of Alfvén waves from the equatorial plane to the 70° (75°) ionosphere along the magnetic field lines. Considering this time delay, the vorticity distribution in Figure 3 almost corresponds to the electric potential distribution at the ionosphere in Figure 2. It is worthwhile to note here that the distribution of the vorticity itself shows the skew in the equatorial plane. The longer Alfvén transit time in higher latitudes also enhances the skew of the TCVs in the ionosphere. In terms of the position of the source current of the field-aligned currents driving the simulated TCVs, we regard that the magnetopause current has a minor importance because of two reasons. First, there is small field-aligned current near the open/close boundary at the ionospheric latitude of ~80° compared with the one of ~75° in Figure 2. The second reason is that the Alfvén transit time from the equatorial magnetopause to the ionosphere is too long (5–8 min) to become the effective source of the simulated TCVs.

5. Wave Equation of Field-Aligned Currents

[16] Sections 3 and 4 reveal the correspondence between the ionospheric potential and the vorticity in the magnetosphere. However, the exact generation mechanism of field-aligned currents associated with TCVs remains an open question. It is possible to answer the question quantitatively by using the full four-dimensional time-space data obtained through the simulation. However, in the realistic ambient magnetic field and plasma environment, it is difficult to analyze the magnetospheric disturbances when we use the former theoretical approaches developed under a simplified condition. The formula suitable for such analysis is the wave equation of field-aligned currents proposed by *Itonaga et al.* [2000]. We introduce the wave equation to evaluate the generation mechanism of field-aligned currents in detail.

$$\frac{1}{V_{\mathrm{A}}^2}\frac{\partial^2 \delta j_{\parallel}}{\partial t^2} - \frac{1}{V_{\mathrm{A}}^2}\frac{\partial}{\partial s}\left[V_{\mathrm{A}}^2 B \frac{\partial}{\partial s}\left(\frac{\delta j_{\parallel}}{B}\right)\right] = \mathrm{T1} + \mathrm{T2} + \mathrm{T3} + \mathrm{T4} \quad (1)$$

$$\mathrm{T1} = -\frac{1}{V_{\mathrm{A}}^2}\frac{\partial}{\partial s}\left(\nabla V_A^2 \cdot \delta \mathbf{j}_{\mathrm{I}}\right) \quad (2)$$

$$\mathrm{T2} = \frac{1}{V_{\mathrm{A}}^2}\left[\nabla^2\left(V_{\mathrm{A}}^2 \delta \mathbf{j}_{\mathrm{I}}\right)\right]_{\parallel} \quad (3)$$

$$\mathrm{T3} = -\frac{1}{V_{\mathrm{A}}^2}\frac{\partial}{\partial s}\left(\frac{V_{\mathrm{A}}^2}{p_B}\nabla_{\perp} p_B \cdot \delta \mathbf{j}_{\mathrm{D}}\right) \quad (4)$$

$$\mathrm{T4} = -\frac{1}{V_{\mathrm{A}}^2}\frac{\partial}{\partial s}\left(\frac{V_{\mathrm{A}}^2}{2p_B}\nabla_{\perp}(\delta p_B - \delta p) \cdot \mathbf{j}_{\mathrm{D}}\right) \quad (5)$$

$$\delta \mathbf{j}_{\mathrm{I}} = \frac{1}{B^2}\mathbf{B} \times \left(\rho \frac{\partial \delta \mathbf{u}}{\partial t}\right) \quad (6)$$

$$\delta \mathbf{j}_{\mathrm{D}} = \frac{1}{B^2}\mathbf{B} \times (\nabla_{\perp} \delta p) \quad (7)$$

$$\mathbf{j}_{\mathrm{D}} = \frac{1}{B^2}\mathbf{B} \times (\nabla_{\perp} p) \quad (8)$$

The variable s is a distance measured along the magnetic field line and increases in the direction of **B**. The double-parallel subscript stands for a scalar component parallel to **B**. The term $\delta p_B = B\delta B/\mu_0$ is the perturbed magnetic pressure.

[17] As shown in equations (2) and (3), T1 and T2 mean that the perturbed field-aligned current is produced by the perturbed inertia current (equation (6)) where there is inhomogeneity of Alfvén speed or curvature of the magnetic field line, respectively. The third term T3, shown in equation (4), shows that the perturbed field-aligned current is caused by the perturbed diamagnetic current (equation (7)) where the unperturbed magnetic pressure is inhomogeneous. The fourth term T4, shown in equation (5), means that the perturbed field-aligned current is generated by perturbations of the magnetic and plasma pressures where the diamagnetic current (equation (7)) flows in the unperturbed state. Note that the term T1 corresponds to the L96 model, while the terms T3 and T4 are associated with the G92 model. Therefore we can investigate the importance of these proposed models by evaluating these source terms from the simulated results.

[18] Since there are no TCV models discussing the generation of field-aligned currents via the curvilinear effect T2, we explain the meaning in detail. Assume that the ambient magnetic field as $\mathbf{B} = \nabla\Phi \times \nabla\varphi$, where Φ and φ are Euler potentials [*Stern*, 1967], and $\nabla\Phi \cdot \nabla\varphi = 0$ without loss of generality. The Euler potentials Φ and φ are constant along each magnetic field line and label the meridional and longitudinal directions, respectively. When the characteristic length in spatial variation of the perturbed inertial current is much smaller than those of the scale factors of the Euler potentials and the Alfvén speed, we can approximate the term T2 in a simple form [*Itonaga et al.*, 2000]

$$\frac{1}{V_{\mathrm{A}}^2}\left[\nabla^2\left(V_{\mathrm{A}}^2 \delta \mathbf{j}_{\mathrm{I}}\right)\right]_{\parallel} \sim \frac{2}{R_{\mathrm{c}}}\frac{\partial \delta j_{\Phi}}{\partial s}, \quad (9)$$

where R_{c} denotes the radius of curvature of the magnetic field line designated by Φ. Equation (9) means that the curvilinear effect is enhanced when perturbed inertial currents in the curvature direction vary along with the magnetic field line in the case that there is a significant curvature. Therefore the main source current of the curvilinear effect is the curvature component of the perturbed inertial current.

[19] In order to evaluate each source term in equation (1), we need to calculate perturbed values of MHD parameters. The perturbed values are defined as their deviations from those before the solar wind impulse at 2.1 min. The

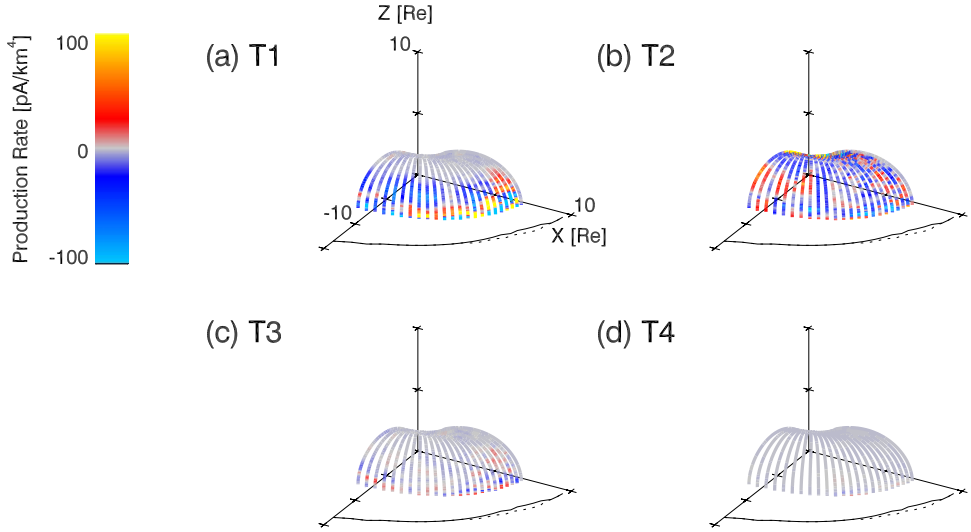

Figure 4. Three-dimensional view of the magnetic field lines originated from the ionospheric latitude of 70°. The magnetopause positions at 2.1 min and 3.0 min are depicted on the equatorial plane as dotted and solid lines, respectively. Warm and cold colors denote positive and negative amplitudes of the four source terms in the wave equation (1).

perturbed inertia current (equation (6)) is evaluated based on the following equation:

$$\rho \frac{\partial \delta \mathbf{u}}{\partial t} = (\mathbf{j} + \delta \mathbf{j}) \times (\mathbf{B} + \delta \mathbf{B}) - \nabla (p + \delta p). \qquad (10)$$

Spatial derivatives are approximated by a central difference in spherical coordinates.

6. Discussion

[20] Now we investigate how the dominant field-aligned currents are excited in the magnetospheric source regions mapped to ionospheric latitudes of 70° and 75°. These field-aligned currents are associated with the strong perturbed flow shear as shown in Figure 3. Figures 4 and 5 show the three-dimensional view of the magnetic field lines originated from the ionospheric latitudes of 70° and 75°, respectively. The circles in Figures 2 and 3 are the footprints of these magnetic field lines at both ends. Figures 4 and 5 have the same format and the same color scale for comparisons. The magnetopause positions at 2.1 min and 3.0 min are depicted as dotted and solid lines, respectively. Results are shown as snapshots at 3.0 min. The generation mechanism discussed hereafter is essentially the same even after 3.0 min, although the amplitude decays.

[21] On the 70° latitude field lines, the diamagnetic terms T3 and T4 are negligible as shown in Figures 4c and 4d. Figures 4a and 4b show that around the LT sector of the magnetopause ripple, the inhomogeneous effect T1 is dom-

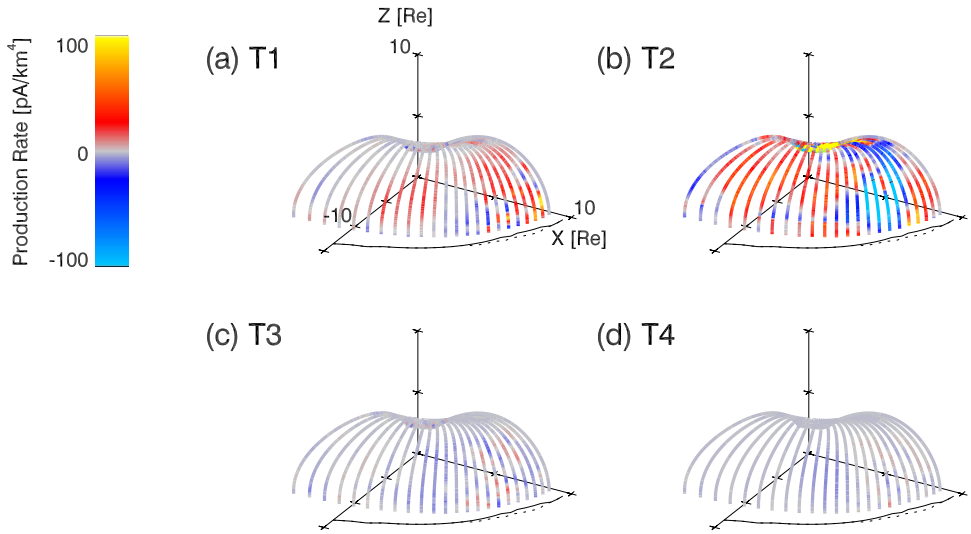

Figure 5. Three-dimensional view of the magnetic field lines originated from the ionospheric latitude of 75°. The format and color scale are the same as Figure 4.

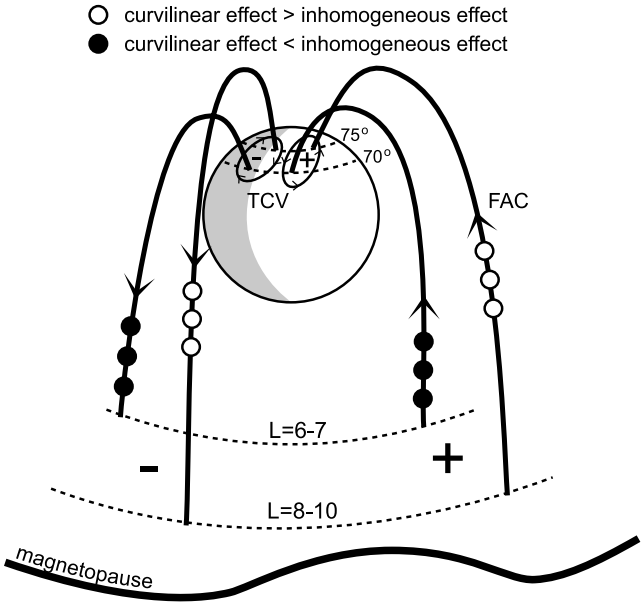

Figure 6. Summary sketch to describe the generation mechanism of field-aligned currents caused by a localized density pulse in the solar wind.

inant near the equatorial region, while the curvilinear effect T2 is dominant off from the equatorial region. This inhomogeneous effect T1 is interpreted by the mode conversion from compressional wave to shear Alfvén wave that occurs in the inner equatorial region of $6 < L < 7$ where the radial gradient of Alfvén speed is enhanced as explained by *Fujita et al.* [2003].

[22] On the 75° latitude field lines, the diamagnetic terms T3 and T4, are negligible as seen in Figures 5c and 5d. The inhomogeneous effect T1 is not dominant as shown in Figure 5a because of a lack of sharp gradient of Alfvén speed. As shown in Figure 5b, the curvilinear effect T2 is dominant off from the equatorial plane in the LT sector of the magnetopause ripple. The curvilinear effect appearing in Figures 4b and 5b does not mean the mode conversion but is interpreted by the conversion of polarization current into the field-aligned current within the shear Alfvén mode.

[23] Let us summarize the evaluation of the generation mechanisms of field-aligned currents discussed above. The field-aligned currents driving the simulated TCVs are mainly generated in the magnetospheric region of $6 < L < 10$ with the inner and outer boundaries mapped to the ionospheric latitudes of 70° and 75°, respectively. The magnetopause, dealt by the KS91 and G92 models, is not identified as the main source region. The field-aligned currents produced in the KS91 and G92 models may be discriminated when the magnetopause ripple is much amplified, for example, as shown by *Sibeck et al.* [1999]. Simulations using several different types of solar wind drivers are very interesting as a next step. The field-aligned current suggested by the L96 model is not identified in the outer region mapped to the ionospheric latitude of 75°, although the mode conversion takes place in the inner region mapped to the ionospheric latitude of 70°. This is because the LLBL plasma in our simulation is not included as proposed by the L96 model. In the real magnetosphere, however, the field-aligned current of the L96 model would be enhanced in the outer magnetosphere because of sharp gradient of Alfvén speed at the inner edge of the LLBL.

[24] Figure 6 shows an illustration summarizing the dominant generation mechanism of pairs of field-aligned currents due to a localized density pulse. The magnetopause is deformed by the localized impact, and a ripple structure moves antisunward. In-out plasma acceleration accompanied with the magnetopause deformation causes the inertia current, and the vorticity arises in the magnetosphere. Since the vorticity is approximately equivalent to the electric charge, discharge occurs via field-aligned currents in two ways. In the magnetospheric region of $8 < L < 10$ the inertial current is converted into the field-aligned current off from the equatorial plane via the curvilinear effect. On the other hand, in the magnetospheric region of $6 < L < 7$ where the sharp gradient of Alfvén speed exists, the inertia current is converted into the field-aligned current not only by the curvilinear effect but also via the inhomogeneous effect.

7. Conclusion

[25] TCVs are reproduced by a MHD simulation of the transient response of the magnetosphere-ionosphere system to a localized density pulse in the solar wind. Dominant source of the field-aligned currents driving the simulated TCVs are not identified in the magnetopause region. The source of the field-aligned currents is the inertial current associated with in-out plasma acceleration within the magnetosphere near the impact region. The curvilinear effect off from the equatorial region is an important mechanism to produce the field-aligned currents. The inhomogeneous effect also generates the field-aligned currents at sharp gradient of Alfvén speed.

[26] **Acknowledgments.** Numerical calculations were performed by NEC SX6 installed at the Communications Research Laboratory and the Computer Center of the National Institute of Polar Research, as well as the Computer Center of Nagoya University. This work was partly supported by the Japan Society for the Promotion of Science (JSPS) under Grant-in-Aid for Scientific Research 14540415. One of the authors (R. K.) is supported by a grant of JSPS Research Fellowships for Young Scientists.

[27] Lou-Chuang Lee thanks Robert L. Lysak and Yu Lin for their assistance in evaluating this paper.

References

Amm, O., M. J. Engebretson, T. Hughes, L. Newitt, A. Viljanen, and J. Watermann (2002), A traveling convection vortex event study: Instantaneous ionospheric equivalent currents, estimation of field-aligned currents, and the role of induced currents, *J. Geophys. Res.*, *107*(A11), 1334, doi:10.1029/2002JA009472.

Chen, G. X., Y. Lin, and S. Cable (2000), Generation of traveling convection vortices and field-aligned currents in the magnetosphere by response to an interplanetary tangential discontinuity, *Geophys. Res. Lett.*, *27*(21), 3583–3586.

Cowley, S. W. (2000), Magnetosphere-ionosphere interactions: A tutorial review, in *Magnetospheric Current Systems*, *Geophys. Monogr. Ser.*, vol. 118, edited by S. Ohtani et al., pp. 91–106, AGU, Washington, D. C.

Friis-Christensen, E., M. A. McHenry, C. R. Clauer, and S. Vennerstrom (1988), Ionospheric traveling convection vortices observed near the polar cleft: A triggered response to sudden changes in the solar wind, *Geophys. Res. Lett.*, *15*(3), 253–256.

Fujita, S., T. Tanaka, T. Kikuchi, K. Fujimoto, K. Hosokawa, and M. Itonaga (2003), A numerical simulation of the geomagnetic sudden commencement: 1. Generation of the field-aligned current associated with the preliminary impulse, *J. Geophys. Res.*, *108*(A12), 1416, doi:10.1029/2002JA009407.

Glassmeier, K.-H. (1992), Travelling magnetospheric convection twin-vortices: Observations and theory, *Ann. Geophys.*, *10*, 547–565.

Glassmeier, K.-H., M. Hönisch, and J. Untiedt (1989), Ground-based and satellite observations of traveling magnetospheric convection twin vortices, *J. Geophys. Res.*, *94*(A3), 2520–2528.

Itonaga, M., A. Yoshikawa, and S. Fujita (2000), A wave equation describing the generation of field-aligned current in the magnetosphere, *Earth Planets Space*, *52*, 503–507.

Kataoka, R., H. Fukunishi, L. J. Lanzerotti, C. G. Maclennan, H. U. Frey, S. B. Mende, J. H. Doolittle, T. J. Rosenberg, and A. T. Weatherwax (2001), Magnetic impulse event: A detailed case study of extended ground and space observations, *J. Geophys. Res.*, *106*(A11), 25,873–25,890.

Kataoka, R., H. Fukunishi, L. J. Lanzerotti, T. J. Rosenberg, A. T. Weatherwax, M. J. Engebretson, and J. Watermann (2002), Traveling convection vortices induced by solar wind tangential discontinuities, *J. Geophys. Res.*, *107*(A12), 1455, doi:10.1029/2002JA009459.

Kataoka, R., H. Fukunishi, K. Hosokawa, H. Fujiwara, A. S. Yukimatu, N. Sato, and Y.-K. Tung (2003a), Transient production of F region irregularities associated with TCV passage, *Ann. Geophys.*, *21*, 1531–1541.

Kataoka, R., H. Fukunishi, and L. J. Lanzerotti (2003b), Statistical identification of solar wind origins of magnetic impulse events, *J. Geophys. Res.*, *108*(A12), 1436, doi:10.1029/2003JA010202.

Kivelson, M. G., and D. J. Southwood (1991), Ionospheric traveling vortex generation by solar wind buffering of the magnetosphere, *J. Geophys. Res.*, *96*(A2), 1661–1667.

Lanzerotti, L. J., R. M. Konik, and A. Wolfe (1991), Cusp latitude magnetopause events: 1. Occurrence statistics, *J. Geophys. Res.*, *96*(A8), 14,009–14,022.

Lühr, H., and W. Blawert (1994), Ground signatures of traveling convection vortices, in *Solar Wind Sources of Magnetospheric Ultra-Low-Frequency-Waves*, *Geophys. Monogr. Ser.*, vol. 81, edited by M. J. Engebretson, K. Takahashi, and M. Scholer, pp. 231–251, AGU, Washington, D. C.

Lühr, H., M. Lockwood, P. E. Sandholt, T. L. Hansen, and T. Moretto (1996), Multi-instrument ground-based observations of a travelling convection vortices event, *Ann. Geophys.*, *14*, 162–181.

Lysak, R. L., and D. Lee (1992), Response of the dipole magnetosphere to pressure pulses, *Geophys. Res. Lett.*, *19*(9), 937–940.

Moretto, T., and A. Yahnin (1998), Mapping travelling convection vortex events with respect to energetic particle boundaries, *Ann. Geophys.*, *16*, 891–899.

Moretto, T., E. Friis-Christensen, H. Lühr, and E. Zesta (1997), Global perspective of ionospheric traveling convection vortices: Case studies of two Geospace Environmental Modeling events, *J. Geophys. Res.*, *102*(A6), 11,597–11,610.

Murr, D. L., and W. J. Hughes (2003), Solar wind drivers of Traveling Convection Vortices, *Geophys. Res. Lett.*, *30*(7), 1354, doi:10.1029/2002GL015498.

Murr, D. L., W. J. Hughes, A. S. Rodger, E. Zesta, H. U. Frey, and A. T. Weatherwax (2002), Conjugate observations of traveling convection vortices: The field-aligned current system, *J. Geophys. Res.*, *107*(A10), 1306, doi:10.1029/2002JA009456.

Sibeck, D. G., et al. (1999), Comprehensive study of the magnetospheric response to a hot flow anomaly, *J. Geophys. Res.*, *104*(A3), 4577–4593.

Sibeck, D. G., R. B. Decker, D. G. Mitchell, A. J. Lazarus, R. P. Lepping, and A. Szabo (2001), Solar wind preconditioning in the flank foreshock: IMP8 observations, *J. Geophys. Res.*, *106*(A10), 21,675–21,688.

Sibeck, D. G., N. B. Trivedi, E. Zesta, R. B. Decker, H. J. Singer, A. Szabo, H. Tachihara, and J. Watermann (2003), Pressure-pulse interaction with the magnetosphere and ionosphere, *J. Geophys. Res.*, *108*(A2), 1095, doi:10.1029/2002JA009675.

Slinker, S. P., J. A. Fedder, W. J. Hughes, and J. G. Lyon (1999), Response of the ionosphere to a density pulse in the solar wind: Simulation of traveling convection vortices, *Geophys. Res. Lett.*, *26*(23), 3549–3552.

Stern, D. (1967), Geomagnetic Euler potentials, *J. Geophys. Res.*, *72*(15), 3995–4005.

Tanaka, T. (1994), Finite Volume TVD scheme on an unstructured grid system for three-dimensional MHD simulation of inhomogeneous systems including strong background potential fields, *J. Compt. Phys.*, *111*, 381–389.

Tanaka, T. (1995), Generation mechanisms for magnetosphere-ionosphere current systems deduced from a three-dimensional MHD simulation of the solar wind-magnetosphere-ionosphere coupling processes, *J. Geophys. Res.*, *100*(A7), 12,057–12,074.

Tanaka, T. (1999), Configuration of the magnetosphere-ionosphere convection system under northward IMF conditions with nonzero IMF B_y, *J. Geophys. Res.*, *104*(A7), 14,683–14,690.

Tanaka, T. (2000a), The state transition model of the substorm onset, *J. Geophys. Res.*, *105*(A9), 21,081–21,096.

Tanaka, T. (2000b), Field-aligned current systems in the numerically simulated magnetosphere, in *Magnetospheric Current Systems*, *Geophys. Monogr. Ser.*, vol. 118, edited by S.-I. Ohtani et al., p. 53–59, AGU, Washington, D. C.

S. Fujita, Meteorological College, Kashiwa, 277-0852, Japan.

H. Fukunishi and R. Kataoka, Department of Geophysics, Tohoku University, Sendai, 980-8578, Japan. (ryuho@pat.geophys.tohoku.ac.jp)

M. Itonaga, Faculty of Education, Yamaguchi University, Yamaguchi, 753-8513, Japan.

T. Tanaka, Graduate School of Sciences, Kyushu University, Fukuoka, 812-8581, Japan.